Effects of finite element formulation on optimal plate and shell structural topologies

Craig S. Long *, Philip W. Loveday, and Albert A. Groenwold

Abstract

The effects of selected membrane, plate and flat shell finite element formulations on optimal topologies are numerically investigated. Two different membrane components are considered. The first is a standard 4-node bilinear quadrilateral, and the other is a 4-node element accounting for in-plane (drilling) rotations. Plate elements selected for evaluation include discrete Kirchhoff quadrilateral (DKQ) element as well as two Mindlin-Reissner based elements, one employing selective reduced integration (SRI), and the other an assumed natural strain (ANS) formulation. The flat shell elements consist of an assemblage of these membrane and plate components. Both Mindlin-Reissner elements are shown to recover the thin plate result computed using DKQ elements for popular benchmark topology optimization plate problems. However, a new benchmark problem is introduced illustrating the deficiencies of Mindlin-Reissner elements employing SRI on transverse shear terms. For shell problems, elements which properly account for in-plane rotations are shown to be insensitive to the penalty parameter which enforces the relationship between in-plane rotations and displacements, in contrast to the situation when an *ad hoc* treatment of drilling degrees of freedom is used.

Key words: finite element formulation, topology optimization

1 Introduction

Due to its potential to automatically generate not only good, but optimal designs, topology optimization has been receiving unprecedented attention of late. However, we believe that an aspect of the problem which has not received sufficient attention is the effect of the the actual finite element approximation employed, on the resulting optimal topology.

* Sensor Science & Technology, CSIR Material Science & Manufacturing, Box 395, Pretoria, South Africa, 0001. Tel.: +27-12-8412498. Fax: +27-12-8413895.
Email address: clong@csir.co.za (Craig S. Long).

In this work the popular SIMP (Simple Isotropic Material with Penalization) material parametrization is employed in order to demonstrate the effect of element selection in structural topology optimization. The possibility of a SIMP-like method was originally mentioned by Bendsøe [1], (although, based on theoretical grounds, a preference for homogenization methods was expressed). Rozvany and Zhou [2] and the University of Essen research group must, however, also be credited for independently suggesting and significantly popularizing SIMP over the years. In fact, the term "SIMP" was coined by Rozvany *et al.* [3]. For a more detailed history of SIMP, the reader is referred to [4] or [5].

It should be noted, that 'optimal' topologies are known to be a function of the topology optimization algorithmic settings [6]. Therefore, it is not guaranteed that the *global* optimal of the evaluated problems are necessarily reported here. Having said that, the optimal topologies presented herein closely resemble previously reported results, where comparison is possible. Furthermore, where appropriate, the actual compliance of the topologies are compared quantitatively to avoid simply comparing topologies visually.

Special attention is paid to plate and shell problems and it is therefore appropriate to give some background on structural topology optimization of plate and shell problems at this point. There has been a plethora of work in this field, so this is by no means an exhaustive review of all work done. A more thorough review can be found in, for example the book of Bendsøe and Sigmund [7].

Tenek and Hagiwara [8] employed homogenization techniques to generate optimal isotropic single layer and multilayer anisotropic plate topologies. The finite elements used in their work are based on Mindlin-Reissner plate theory, and are four noded bilinear quadrilateral elements with only 5 degrees of freedom (DOFs) per node (the in-plane rotation is omitted since only flat problems are considered). This work was extended by Tenek and Hagiwara [9] considering the topology optimization of plates, as well as single and doubly curved shell structures. Strain energy was minimized subject to a volume constraint. Again, simple four noded quadrilateral elements with 5 DOFs per node were employed with selective reduced integration (SRI) to alleviate shear locking.

There are of course numerous other authors who have used homogenization methods to solve topology optimization problems for plate and shell structures, for example see Díaz *et al.* [10], Krog and Olhoff [11], or see Bendsøe and Sigmund [7] for a more complete list of references.

Recently Hinton and co-workers [6,12] have addressed the topology optimization problem of plate and shell structures using SIMP-like material models. The Mindlin-Reissner based element used in their work is detailed in [13], and

employs SRI on shear terms to overcome transverse shear locking. Since then SIMP-like material parametrizations have become very popular in this type of problem, see for example Pedersen [14], Jog [15] (who implement the MITC4 and MITC9 elements of Bathe and co-workers [16]) and Stegmann and Lund [17], who also use MITC elements.

Meanwhile, many advances have been made in finite element technology, which have a direct bearing on structural topology optimization, since most of the applications in topology optimization employ the finite element method as an analysis tool. As mentioned previously however, little attention is usually paid to the actual finite element formulation in the application.

As is customary in topology optimization, we employ flat shell finite elements (assembly of plate and membrane elements) in the analysis of generally curved shell structures. These elements can only be effective if the membrane and plate components from which they are constructed, are independently accurate and robust.

Two membrane components are considered. The first is an isoparametric 4-node bilinear quadrilateral [18]. The other is a 4-node element accounting for in-plane (drilling) rotations based on the variational framework set out by Hughes and Brezzi [19]. Plate elements selected for evaluation include the discrete Kirchhoff quadrilateral (DKQ) element, see for example [20], as well as two Mindlin-Reissner based elements, one employing selective reduced integration (SRI) [21], and the other an assumed natural strain (ANS) formulation [22,23].

Further details of the finite element formulations considered are presented in some detail in Section 3 and will therefore not be repeated here.

2 Topology optimization problem formulation

In this section, a very brief discussion of the topology optimization formulation used for evaluation, is presented. The minimum compliance problem is specifically focused on. Some details of the material parametrization of multilayer designs are given. Also presented is a very short description of the optimality criteria based updating scheme employed, as well as the filtering strategy employed to address the mesh dependency problem.

2.1 Material parametrization

The discretized finite element model is parameterized using the popular Simple Isotropic Material with Penalization (SIMP) method [7], in which material properties are scaled with an artificial density parameter ρ, with $0 \leq \rho \leq 1$ raised to a power p (usually $1 < p \leq 6$), representing a penalty exponent which renders intermediate densities uneconomical.

As in Lee *et al.* [6] and Stegmann and Lund [17] numerical experiments with multilayer shell structures are performed. Figure 1 schematically shows the problem considered. The constitutive relations are computed using classical laminate theory by analytical through-thickness integration. For the isotropic materials used in this study, the stress resultant form of the constitutive equations can be calculated by pre-integration through the thickness. Thus for for a laminate of thickness h with N_l layers, the relations between the stress resultants and strains for multilayer shells can be expressed, as in [6], as:

$$\begin{Bmatrix} \boldsymbol{N} \\ \boldsymbol{M} \\ \boldsymbol{Q} \end{Bmatrix} = \begin{bmatrix} \boldsymbol{\mathcal{A}}(\boldsymbol{\rho}) & \boldsymbol{\mathcal{B}}(\boldsymbol{\rho}) & \mathbf{0} \\ \boldsymbol{\mathcal{B}}(\boldsymbol{\rho}) & \boldsymbol{\mathcal{D}}(\boldsymbol{\rho}) & \mathbf{0} \\ \mathbf{0} & \mathbf{0} & \boldsymbol{\mathcal{G}}(\boldsymbol{\rho}) \end{bmatrix} \begin{Bmatrix} \boldsymbol{\epsilon}_{\mathrm{m}} \\ \boldsymbol{\kappa} \\ \boldsymbol{\gamma} \end{Bmatrix}, \tag{1}$$

where $\boldsymbol{\epsilon}_{\mathrm{m}}$, $\boldsymbol{\kappa}$ and $\boldsymbol{\gamma}$ are the membrane, bending and transverse shear strains respectively and $\boldsymbol{N}$, $\boldsymbol{M}$ and $\boldsymbol{Q}$ are the corresponding stress resultants. The specific forms of the constitutive submatrices $\boldsymbol{\mathcal{A}}(\boldsymbol{\rho})$, $\boldsymbol{\mathcal{B}}(\boldsymbol{\rho})$, $\boldsymbol{\mathcal{D}}(\boldsymbol{\rho})$, $\boldsymbol{\mathcal{G}}(\boldsymbol{\rho})$ in (1), may be found in [6]. The artificial density of layer i may be denoted ρ_i. Note that layers that are *a priori* solid or void, and therefore do not form part of the design problem, are simply accounted for by setting $\rho_i = 1$ for solid layers or $\rho_i = \rho_{\min}$ for void layers. The vector containing the density in the N_l layers is denoted $\boldsymbol{\rho}$.

Minimum compliance topology optimization problems impose a constraint on the amount of material which can be utilized. The volume of a given element can be computed (assuming a constant area A through the thickness) as

$$V_e(\boldsymbol{\rho}) = \int_{-\frac{h}{2}}^{\frac{h}{2}} A(\boldsymbol{\rho}) \mathrm{d}z = \sum_{i=1}^{N_l} \rho_i \; A(z_{i+1} - z_i). \tag{2}$$

The volume of the entire structure is then easily computed as the sum of all element volumes:

$$V = \sum_{e=1}^{N_{el}} V_e, \tag{3}$$

where N_{el} represents the total number of elements in the assembly. In this work the design volume, or the volume of the design domain, will also be

referred to. This is calculated as the difference between the total volume (3) and the volume of the elements or layers which are prescribed to be solid or void. In other word, the design volume is the volume of all the layers which are a function of the design variables (artificial densities).

2.2 Layer models

Numerous laminate material models are possible using the material parametrization described in Section 2.1. For the purposes of this paper, only symmetric material models will be considered, implying no coupling between membrane and bending actions since $\mathcal{B} = \mathbf{0}$. Specifically, the two layer models considered are the:

- Single layer material model. This represents the classical topology optimization problem for plate and shell problems, and allows for the introduction of holes through the entire thickness (perforated plates/shells).
- Three layer ribbed or rib stiffened material model. This model maintains an inner layer which is *a priori* solid with outer layers consisting of artificial material, allowing for the introduction of stiffening zones symmetric to the shell mid-surface.

2.3 Problem formulation and sensitivities

The conventional minimum compliance topology optimization problem is considered. This problem may be written in standard form as

$$\min_{\boldsymbol{\rho}} c(\boldsymbol{\rho}) \tag{4}$$

$$\text{such that} : \sum_{e=1}^{N_{el}} V_e \leq V^*, \tag{5}$$

$$: \boldsymbol{K}\boldsymbol{Q} = \boldsymbol{F}, \tag{6}$$

$$: 0 < \rho_{\min} \leq \rho_e \leq 1, \quad e = 1, 2, \ldots, N_{el} \tag{7}$$

where c is the compliance given by $c(\boldsymbol{\rho}) = \boldsymbol{F}^T\boldsymbol{Q}(\boldsymbol{\rho})$, and where the displacements, $\boldsymbol{Q}$, are determined from $\boldsymbol{K}(\boldsymbol{\rho})\boldsymbol{Q}(\boldsymbol{\rho}) = \boldsymbol{F}$. In this problem, the force vector $\boldsymbol{F}$ is independent of the artificial density. The allowable volume is denoted V^*. The sensitivity of the linear volume constraint in (5) can easily be determined. The sensitivity of the compliance (4) can be calculated using the adjoint method [7]. Note that in the treatment above, each element e in the finite element mesh has only one corresponding density variable ρ_e. In the case of the three layer stiffening model, for example, this variable scales the material properties of the two outer layers simultaneously.

2.4 Design update and filtering strategies

The design update is carried out using the standard fixed-point updating scheme based on the conditions of optimality [7]. The standard algorithmic parameters are used, i.e. a move limit of $\zeta = 0.2$ and a value of $\eta = \frac{1}{2}$ for the 'tuning' parameter which numerically damps the oscillatory nature of the algorithm. The aforementioned settings are used for all results presented herein. In this way, the effect of element formulation on optimal topology is isolated.

The final implementational issue is that of mesh dependency. In order to overcome this problem, as well as the checkerboarding problem (see [7,24,25] for details) the sensitivity filtering method of Sigmund [25] is used, with a filter radius of 1.2 element side lengths in all cases.

3 Finite element formulations

In this section, the formulations of the various shell finite elements used in the numerical experiments, are briefly outlined. Each shell finite element, with associated elemental displacements and rotations, can be decomposed as

$$\boldsymbol{k}\,\boldsymbol{q} = \begin{bmatrix} \boldsymbol{k}_{\mathrm{m}} & \boldsymbol{k}_{\mathrm{mp}} \\ \boldsymbol{k}_{\mathrm{mp}}^{T} & \boldsymbol{k}_{\mathrm{p}} \end{bmatrix} \begin{Bmatrix} \boldsymbol{q}_{\mathrm{m}} \\ \boldsymbol{q}_{\mathrm{p}} \end{Bmatrix}, \tag{8}$$

where $\boldsymbol{k}$ represents the stiffness matrix in a locally defined coordinate system, with related local nodal displacements and rotations $\boldsymbol{q}$. The partitioned membrane and plate stiffness matrices are denoted $\boldsymbol{k}_{\mathrm{m}}$ and $\boldsymbol{k}_{\mathrm{p}}$, respectively. The coupling stiffness between membrane and plate actions is denoted $\boldsymbol{k}_{\mathrm{mp}}$.

The associated local displacements $\boldsymbol{q}$ are decomposed into terms associated with membrane actions, $\boldsymbol{q}_{\mathrm{m}}$, and those associated with the plate component, $\boldsymbol{q}_{\mathrm{p}}$. Specifically, $\boldsymbol{q}_{\mathrm{m}} = [\boldsymbol{u}\ \boldsymbol{v}\ \boldsymbol{\theta}_z]^T$, where $[\boldsymbol{u}\ \boldsymbol{v}]^T$ represent the in-plane nodal displacements only, and $\boldsymbol{\theta}_z$ denotes the in-plane rotations or drilling DOFs at each node. The plate transverse displacement and rotations are given by $\boldsymbol{q}_{\mathrm{p}} = [\boldsymbol{w}\ \boldsymbol{\theta}_x\ \boldsymbol{\theta}_y]^T$.

For clarity, some detail of the membrane and plate components of the elemental stiffness matrix are now presented separately in the local coordinate system.

3.1 Membrane elements

Two membrane finite element formulations are employed. The first is the traditional Q4 displacement-based element which neglects in-plane rotations. The rotations can, however, be accommodated by an extremely simple, but *ad hoc* treatment. This method has no theoretical basis, and is used to illustrate the pitfalls of an improper treatment of element deficiencies.

The second membrane element is based on the variational formulation due to Hughes and Brezzi [19], with the finite element implementation investigated by Ibrahimbegovic *et al.* [26]. This formulation is based on a rigorous mathematical foundation, and represents a robust, accurate membrane element.

3.1.1 Standard displacement based membrane element

The first membrane element is the standard displacement-based quadrilateral element with bilinear displacement interpolations, see for example [18].This element formulation neglects the in-plane rotational field, θ_z, and possesses only two degrees of freedom per node. A method which is sometimes used to account for the in-plane rotation is simply to add a small fictitious stiffness to each drilling DOF. In this case, this is done by simply replacing the on-diagonal 4×4 null matrix relating to the drilling DOFs, with the matrix $\boldsymbol{k}_{\theta z}$. The stiffness matrix for this membrane element is therefore given by:

$$\boldsymbol{k}_{\mathrm{m}}^{\mathrm{Q4}\alpha} = \begin{bmatrix} \boldsymbol{k}_{\mathrm{m}}^{\mathrm{Q4}} & \boldsymbol{0}_{8\times 4} \\ \boldsymbol{0}_{4\times 8} & \boldsymbol{k}_{\theta z} \end{bmatrix}, \tag{9}$$

where $\boldsymbol{k}_{\theta z}$ is computed by appending the potential energy expression of each element as follows:

$$\Pi^* = \Pi + \int_\Omega \alpha E(\rho) t \, (\theta_z - \bar{\theta}_z)^2 \, \mathrm{d}\Omega, \tag{10}$$

where α is a fictitious elastic parameter, and $\bar{\theta}_z$ is the mean rotation of each element [21,27]. $E(\rho)$ is the elastic modulus which is a function of the element artificial density. As in Cook *et al.* [18] the added matrix provides each drilling DOF with a fictitious stiffness, but offers no resistance to the mode $\theta_z^1 = \theta_z^2 = \theta_z^3 = \theta_z^4$, or any other rigid mode. Some experimentation is usually necessary in order to select a suitable value of α, but if high precision computer code is employed, usually small values of α are recommended [27].

3.1.2 Membrane element with drilling DOFs

The second membrane element accounts for in-plane rotations based on their continuum mechanics definition. The approach relies on a variational formulation employing an independent rotation field, as presented by Hughes and Brezzi [19]. Employing a notation similar to that in [26], the resulting stiffness matrix is given by:

$$\boldsymbol{k}_{\mathrm{m}}^{\mathrm{Q4}\gamma} = \tilde{\boldsymbol{k}}_{\mathrm{m}}^{\mathrm{Q4}\gamma} + \boldsymbol{p}_{\mathrm{m}}^{\gamma}, \tag{11}$$

where $\tilde{\boldsymbol{k}}_{\mathrm{m}}^{\mathrm{Q4}\gamma}$ is a 12×12 matrix given by:

$$\tilde{\boldsymbol{k}}_{\mathrm{m}}^{\mathrm{Q4}\gamma} \;=\; \int_A \left[\boldsymbol{B}_{\mathrm{m}}^{\mathrm{Q4}\gamma} \;\; \boldsymbol{G}_{\mathrm{m}}^{\mathrm{Q4}\gamma}\right]^T \boldsymbol{\mathcal{A}}(\rho) \left[\boldsymbol{B}_{\mathrm{m}}^{\mathrm{Q4}\gamma} \;\; \boldsymbol{G}_{\mathrm{m}}^{\mathrm{Q4}\gamma}\right] \mathrm{d}A, \tag{12}$$

and where $\boldsymbol{p}_{\mathrm{m}}^{\gamma}$ is given by:

$$\boldsymbol{p}_{\mathrm{m}}^{\gamma} \;=\; \gamma(\rho) \int_A \begin{Bmatrix} \boldsymbol{b}_{\mathrm{m}}^{\mathrm{Q4}\gamma} \\ \boldsymbol{g}_{\mathrm{m}}^{\mathrm{Q4}\gamma} \end{Bmatrix} \left[\boldsymbol{b}_{\mathrm{m}}^{\mathrm{Q4}\gamma} \;\; \boldsymbol{g}_{\mathrm{m}}^{\mathrm{Q4}\gamma}\right] \mathrm{d}A \tag{13}$$

$$\text{where } \gamma(\rho) = \alpha G(\rho), \tag{14}$$

with G the shear modulus which is a function of the artificial density variable, and α an adjustable parameter as in (10). In their original work, Hughes and Brezzi [19] suggest a value of $\alpha = 1$ (i.e. $\gamma = G$). Again, γ is a function of the element's artificial density ρ. The forms of $\boldsymbol{B}_{\mathrm{m}}^{\mathrm{Q4}\gamma}$, $\boldsymbol{G}_{\mathrm{m}}^{\mathrm{Q4}\gamma}$, $\boldsymbol{b}_{\mathrm{m}}^{\mathrm{Q4}\gamma}$ and $\boldsymbol{g}_{\mathrm{m}}^{\mathrm{Q4}\gamma}$ can be found in, for example [26,28].

3.2 Plate elements

In the numerical study to follow, three different plate elements are employed. The first is the popular discrete Kirchhoff quadrilateral (DKQ) element based on the Kirchhoff assumptions for thin plates, in which transverse shear is neglected. The other two elements are Mindlin-Reissner based elements, and differ only in the way in which shear locking is overcome.

3.2.1 Discrete Kirchhoff quadrilateral plate element

DKQ plate elements are commonly used in the analysis of thin plate problems. Since transverse shear deformation (TSD) is not permitted this plate, and of course the resulting shell, is transversely shear rigid. The formulation of the DKQ element is well known, and will therefore not be presented in detail here.

The stiffness matrix of the DKQ element is defined in the standard manner

for displacement models as

$$\boldsymbol{k}_{\mathrm{p}}^{\mathrm{DKQ}} = \int_A [\boldsymbol{B}_{\mathrm{b}}^{\mathrm{DKQ}}]^T \boldsymbol{\mathcal{D}}(\rho) \boldsymbol{B}_{\mathrm{b}}^{\mathrm{DKQ}} \mathrm{d}A, \tag{15}$$

where the specific form of $\boldsymbol{B}_{\mathrm{b}}^{\mathrm{DKQ}}$ can be found in, for example Batoz and Tahar [20] and the bending rigidity matrix $\boldsymbol{\mathcal{D}}(\rho)$ is a function of the artificial density ρ.

3.2.2 Mindlin-Reissner plate element with selective reduced integration

Two Mindlin-Reissner plate elements, based on first order shear deformation theory are evaluated. Assuming independent bilinear interpolations for the transverse displacement and section rotations, the resulting stiffness matrix for a Mindlin-Reissner plate element can be written as

$$\boldsymbol{k}_{\mathrm{p}}^{\mathrm{MR}} = \boldsymbol{k}_{\mathrm{b}}^{\mathrm{MR}} + \boldsymbol{k}_{\mathrm{s}}^{\mathrm{MR}} = \int_A [\boldsymbol{B}_{\mathrm{b}}^{\mathrm{MR}}]^T \boldsymbol{\mathcal{D}}(\rho) \boldsymbol{B}_{\mathrm{b}}^{\mathrm{MR}} \mathrm{d}A + \int_A [\boldsymbol{B}_{\mathrm{s}}^{\mathrm{MR}}]^T \boldsymbol{\mathcal{G}}(\rho) \boldsymbol{B}_{\mathrm{s}}^{\mathrm{MR}} \mathrm{d}A, \tag{16}$$

where the standard forms of $\boldsymbol{B}_{\mathrm{b}}^{\mathrm{MR}}$ and $\boldsymbol{B}_{\mathrm{s}}^{\mathrm{MR}}$ can be found in, for example [18]. It is well known that full integration of the stiffness matrix terms in (16) results in severe locking for thin plates [16,18,21]. A simple method to overcome the locking phenomenon is to employ a selective reduced integration (SRI) scheme on the shear part of the stiffness matrix $\boldsymbol{k}_{\mathrm{s}}^{\mathrm{MR}}$. This procedure will be employed to calculate the first Mindlin-Reissner plate stiffness matrix, i.e.

$$\boldsymbol{k}_{\mathrm{p}}^{\mathrm{SRI}} = \boldsymbol{k}_{\mathrm{b}}^{\mathrm{MR}} + \tilde{\boldsymbol{k}}_{\mathrm{s}}^{\mathrm{MR}}, \tag{17}$$

where $\boldsymbol{k}_{\mathrm{b}}^{\mathrm{MR}}$ is calculated using a 4-point scheme and $\tilde{\boldsymbol{k}}_{\mathrm{s}}^{\mathrm{MR}}$ is evaluated using a single point integration scheme. A potential problem with this method of overcoming locking due to the parasitic shear, is the introduction of spurious zero-energy modes. Two spurious modes are introduced if SRI is employed, one of which is not communicable. Hourglass control, e.g. see [29], will not be used in order to demonstrate how this mode becomes problematic in topology optimization problems.

3.2.3 Mindlin Reissner plate element with assumed natural strain

The second Mindlin-Reissner-based plate element overcomes the effects of shear locking by assuming a mixed interpolation of transverse displacement, section rotations and transverse strains. In particular the assumed natural strain (ANS) formulation of Bathe and Dvorkin [22,23] is considered here. These elements are also called MITC elements (or elements with mixed interpolation of tensorial components). The element of Bathe and Dvorkin has some similarities to the elements of MacNeal [30] and Hughes and Tezduyar [31].

This element has the advantage that it doesn't have any numerically adjustable factors (often required for hourglass control). Furthermore, it contains no spurious zero-energy modes, and passes all appropriate patch tests.

The stiffness matrix derived from this interpolation procedure finally results in the stiffness matrix

$$\boldsymbol{k}_{\mathrm{p}}^{\mathrm{ANS}} = \boldsymbol{k}_{\mathrm{b}}^{\mathrm{MR}} + \boldsymbol{k}_{\mathrm{s}}^{\mathrm{ANS}} = \boldsymbol{k}_{\mathrm{b}}^{\mathrm{MR}} + \int_A [\boldsymbol{B}_{\mathrm{s}}^{\mathrm{ANS}}]^T \boldsymbol{\mathcal{G}}(\rho) \boldsymbol{B}_{\mathrm{s}}^{\mathrm{ANS}} \mathrm{d}A, \tag{18}$$

where the bending part of the stiffness matrix is identical to that of $\boldsymbol{k}_{\mathrm{p}}^{\mathrm{SRI}}$, but the shear part of the stiffness matrix is derived including the ANS interpolations and evaluated using full integration. The strain operator $\boldsymbol{B}_{\mathrm{s}}^{\mathrm{ANS}}$ can be derived as described in [16,22].

3.3 Shell element denotation

Formulations of two membrane and three plate elements have been presented, which allows for a total of six different flat shell elements. The two membrane components are denoted:

- Q4α - The standard Q4 displacement based four node quadrilateral element with the *ad hoc* treatment of drilling DOFs. The Q4α stiffness matrix is given in (9).
- Q4γ - The four node membrane element based on the variational formulation of Hughes and Brezzi [19], and with local stiffness matrix given by (11).

The three plate components are denoted:

- DKQ - The plate element based on the Kirchhoff-Love thin plate assumption of shear rigidity. The stiffness matrix in local coordinates is presented in (15).
- SRI - The irreducible Mindlin-Reissner based element with selective reduced integration on transverse shear terms, and stiffness matrix given by (17).
- ANS - The assumed natural strain plate element based on Mindlin-Reissner assumptions, suggested by Bathe and Dvorkin [22], in which each of the natural strain components is independently interpolated. The elemental plate stiffness matrix is given in (18).

Shell elements will be denoted using first the membrane, followed by the plate designations. For example, the flat shell element made up of Q4α membrane and DKQ plate components will be represented as Q4αDKQ.

Where necessary, the effect of out-of-plane warp is corrected using the so-called 'rigid link correction' of Taylor [32] to transform the nodal variables to

the projected flat element variables.

4 Numerical Examples

The finite element implementations presented in Section 3 are now numerically tested in a SIMP topology optimization setting. A number of popular benchmark problems, which have been used mostly by researchers to verify effectiveness or correctness of implementation, are investigated. Some new problems, which highlight element deficiencies, are also introduced. Only results for plate and shell problems will be presented. In particular, we wish to investigate:

- The difference in optimal topologies generated using elements based on Kirchhoff theory, compared to those using Mindlin-Reissner theory for thick and thin plate structures.
- The effect of employing selective reduced integration (SRI) in Mindlin-Reissner plate elements, compared to mathematically sound and reliable procedures for overcoming shear locking.
- The sensitivity of optimal topologies to parameters related to drilling DOFs in shell structures.

In each numerical experiment, a uniform material distribution which exactly satisfies the volume constraint is chosen as the starting point. A termination criterion based on the number of iterations only, is employed. Therefore the topology computed after 100 iterations will be referred to as the optimal topology. However, in most cases the solution converged well before 100 iterations.

Finally, in some cases numerical deficiencies cause singularities which result in the gradient of strain energy in particular elements to become very close to zero or even positive. In such circumstances, these spurious values are replaced manually by zero. This problem occurs only when SRI plate elements are used, and instances where the correction is made, are explicitly pointed out.

4.1 Plate examples

The geometry, material properties and support conditions for the plate example problems considered are depicted in Figure 2. In the ribbed example to follow, the layup comprises three layers with the outer layers having thickness $\frac{t}{4}$ and a center layer with a thickness of $\frac{t}{2}$, where t is the total thickness of the laminate. For the thick plates, thickness is set to $t = 0.1$ and for the problems considering thin plates $t = 0.01$ is used. These aspect ratios are in line with

those used by Zienkiewicz and Taylor [21] to classify thick and thin plates.

In each plate example, the problem symmetry is exploited by modeling only a quarter of the plate using 900 square elements in total (i.e. a discretization of 30×30). Although only a quarter of the structure is modeled, the full topology is reported. The available volume for the volume constraint is set, in each case, to half of the design volume.

4.1.1 Simply supported plate with center point load

The geometry and constraints for the first plate problem is depicted in Figure 2(a). The problem consists of a square plate which is simply supported, and subjected to a unit point load applied to the center of the plate. For brevity, only single layer results are presented.

The compliance, together with the corresponding optimal topologies are computed as a function of plate thickness for the three different plate elements used in the study. Figure 3(a) depicts the compliance as a function of plate thickness, plotted on a logarithmic scale, for the three different plate elements. From Figure 3(a) it was confirmed that the DKQ optimal compliance results, follow a cubic trend almost exactly with only slight variations due to numerical noise. The optimal topologies corresponding to the thicknesses evaluated, depicted in Figure 4, confirm that the DKQ optimal topologies are insensitive to plate thickness.

Figure 3(b) depicts the results on a linear scale, normalized with respect to the (cubic) DKQ results. At the thin plate limit (t=0.01), very little difference is observed between the compliances calculated using the three different plate elements. The figure suggests that the SRI plate element is less stiff than the ANS element since higher values of compliance are computed at each thickness value, even when topologies are similar. Also indicated on the figure are the thickness ranges over which design changes occur, corresponding to the changes in the slope of the curve. In both cases the design is significantly changed when the compliance of the structure is approximately 1.2 times that of the DKQ result. Since the compliance of the SRI design is greater than that using ANS elements, this point is reached at a lower thickness for the SRI element and does not occur as gradually as the ANS element. Figure 4 depicts the actual topologies corresponding to the points on the curves in Figures 3(a) and 3(b).

The conclusion is therefore that the differences in topology resulting from SRI and ANS elements, is due to the SRI element being 'softer' (in transverse shear) than the ANS element. Since the bending terms are identical, the softer shear terms of the SRI elements offer less resistance and therefore relatively more strain energy is accommodated by these terms.

4.1.2 Corner supported plate subjected to uniform distributed load

In the previous thin plate problem, the ANS and SRI Mindlin-Reissner based elements generate similar optimal topologies for thin plates. However, a problem is now introduced which the SRI element is known to have difficulty solving [33]. The geometry with boundary conditions is depicted in Figure 2(b). It represents a corner supported plate (i.e. transverse displacement is constrained at the four corner nodes only). The applied load in this case is uniformly distributed over the plate surface. Once again, for brevity only results for the thin ribbed material model are presented.

Figure 5 demonstrates that the optimal topologies calculated using the DKQ and ANS elements are, once again, similar. The SRI plate element has severe difficulty in solving this problem. Indeed, many iterations resulted in elements with slightly negative or near zero compliance. As a result, the optimal topology calculated using SRI elements is completely spurious and different to the results from the other two elements results. In order to explain this, the displaced shape of the optimal topology generated using DKQ elements, analyzed using SRI elements is plotted in Figure 6. The hourglass mode which is known to propagate through SRI meshes can clearly be seen.

4.2 Shell examples

Finally, some results of the analysis of thin shell examples are presented. Since the effect of plate formulation on optimal topologies has already been demonstrated, the effect of membrane component, and especially the inclusion of drilling DOFs, in shell elements is now studied. Therefore, in order to ensure that the results are insensitive to plate formulation, only shell elements with shear rigid plate components are evaluated in this subsection. It is thereby guaranteed that only thin shell results are recovered, since DKQ elements are insensitive to plate thickness, as demonstrated in the previous section.

Two problems are presented and are depicted in Figure 7, the first being a cylindrical shell example, which has been studied by several authors [6,17]. The second problem is introduced here to highlight the sensitivity of optimal shell topologies to the treatment of drilling DOFs.

4.2.1 Cylindrical shell

The first shell problem is depicted in Figure 7(a). The geometry, restraints, applied loads and material properties are all depicted in the figure. The symmetry of the problem is again exploited by only modeling one quarter of the structure with a 30×30 discretization. A volume constraint of half of the de-

sign volume is again imposed. Once again, for brevity only single layer results are presented.

Figure 8 depicts the optimal compliance values, together with the corresponding optimal topologies, as a function of scaling parameter α (see (10) for the Q4α membrane component and (14) for the Q4γ component). The figure illustrates that, when employing the Q4αDKQ element, the compliance and corresponding optimal topologies are sensitive to the value of α, especially when α becomes large. In particular, the optimal topology computed with $\alpha = 100$ is distinctly different qualitatively to the topologies corresponding to the other values of α. The notable decrease in compliance at high values of α, when using Q4αDKQ elements, is due to the artificially high stiffness of the drilling DOFs which, due to the curvature, is propagated through the structure. On the other hand, the optimal topologies generated using Q4γDKQ elements are shown to be insensitive to the scaling value of α.

In Table 1 a comparison of the optimal topologies, in terms of their actual compliance, is presented. For each value of α, the compliance of the optimal topology computed using Q4αDKQ elements (analysed using Q4αDKQ elements) is normalised with respect to the compliance of the optimal topology computed using Q4γDKQ elements (again analysed using Q4αDKQ elements). These results are denoted Case 1 in Table 1. A normalised value greater than 1 would therefore indicate that the topology computed using Q4αDKQ elements is sub-optimal, and that the topology computed using Q4γDKQ elements is in fact superior (assuming both structures are analysed using Q4αDKQ elements). The compliance of both topologies for each value of α are similarly computed and normalised using Q4γDKQ elements. These results are denoted Case 2 in Table 1.

From Table 1 it is apparent that, for a given value of α, both optimal topologies computed have similar values of compliance (all values are close to 1) with the possible exception of topologies computed with $\alpha = 10^2$. In this case, the results presented in the table indicate that the optimal topologies for the two different elements, and for this particular value of α, are indeed different and not simply the result of a premature termination in a local optimum. However, having a situation where optimal topology is dependent on element settings (or element selection) is highly undesirable. It is clear from these results that this is not the case when employing the Q4γDKQ element.

4.2.2 Pretwisted shell

The final shell example is depicted in Figure 7(b). The problem is that of a pretwisted beam, which is clamped at the root, with two point loads applied at the vertices opposite the fixed end. The full geometry is modeled with a

40×40 discretization. A volume constraint of half of the design volume is imposed.

Figure 9 depicts the optimal topologies employing Q4αDKQ and Q4γDKQ elements together with the corresponding compliance values. For this problem, the range of values of α for which the Q4αDKQ and Q4γDKQ elements result in similar topologies is much smaller than the cylindrical shell problem. In fact, each value of α result in a different topology when the finite element model employs Q4αDKQ elements. In contrast, the Q4γDKQ element is once again shown to be stable and robust for all tested values of α.

Table 2 presents a comparison of the optimal topologies in terms of their actual compliance, similar to that presented in Table 1. In this case only the topologies in the range $10^{-2} < \alpha < 10^{0}$ have similar values of compliance (even if the topologies are not identical over this range). Once again, the tabulated values suggest that the differences in these optimal topologies are not simply a result of termination in a local minimum, but are in fact different *optimal* topologies. The fact that the compliance and topologies computed using the Q4γDKQ elements are insensitive to the parameter α suggests that a proper treatment of the drilling DOF is essential in shell topology optimization problems.

5 Conclusions

Numerical experiments were performed in order to determine the effect of finite element formulation on plate and shell topology optimization problems. It was shown that, for given topology optimization algorithmic settings, the resultant optimal topology is indeed dependant on element type. Consequently, appropriate care should be taken when selecting both the element type, and element settings, such that the physics of the problem is accurately modelled.

The plate examples presented confirmed that, since the DKQ element is shear rigid, optimal topologies computed using these elements are not sensitive to plate thickness. Elements employing an assumed natural strain (ANS) formulation were shown to be robust and reliable. The ANS elements consistently recovered thin plate results similar to the DKQ results. Mindlin-Reissner elements with selective reduced integration (SRI) on transverse shear terms are shown to be 'softer' in transverse shear than the ANS Mindlin-Reissner based elements and are therefore more sensitive to plate thickness. However, the SRI element possesses a spurious communicable mode which occasionally renders this element unstable. A corner plate example is introduced which illustrates this problem. It is therefore not recommended that SRI plate elements are used in a topology optimization setting, and that ANS plate elements are

used instead.

Finally, the effect of parameters related to drilling DOFs of shell problems were studied. It was shown that optimal topologies computed with elements with drilling degrees of freedom based on sound mathematical theory are insensitive to the penalty parameter over a wide range. On the other hand, elements with an *ad hoc* treatment of drilling degrees of freedom were found to be far more sensitive to adjustable parameters. This sensitivity to the adjustable parameter is furthermore shown to be problem dependent. A new shell example, in the form of a pretwisted beam, is introduced to exemplify this dependence (even at low values of α). A situation where optimal topology is dependent on element settings is, of course, highly undesirable and it is therefore recommended that only elements with a proper treatment of drilling DOFs are used in the analysis of shell topology optimization problems.

References

[1] M.P. Bendsøe. Optimal shape design as a material distribution problem. *Struct. Optim.*, 1:193–202, 1989.

[2] G.I.N. Rozvany and M. Zhou. Applications of the COC algorithm in layout optimization. In H. Eschenauer, C. Matteck, and N. Olhoff, editors, *Engineering Optimization in Design Processes, Proc. Int. Conf. held in Karlsruhe, Germany, Sept. 1990*, pages 59–70. Springer-Verlag, Berlin, 1991.

[3] G.I.N. Rozvany, M. Zhou, and T. Birker. Generalized shape optimization without homogenization. *Struct. Optim.*, 4:250–252, 1992.

[4] G.I.N. Rozvany. Aims, scope, methods, history and unified terminology of computer-aided topology optimization in structural mechanics. *Struct. Multidisc. Optim.*, 21:90–108, 2001.

[5] G.I.N. Rozvany. A critical review of established methods of structural topology optimization. *Struct. Multidisc. Optim.*, 2008. Published online 21 Feb. 2008, DOI 10.1007/s00158-007-0217-0.

[6] S.J. Lee, J.E. Bae, and E. Hinton. Shell topology optimization using layered artificial material model. *Int. J. Numer. Meth. Engng.*, 47:843–867, 2000.

[7] M.P. Bendsøe and O. Sigmund. *Topology Optimization: Theory, Methods and Applications*. Springer, Berlin, 2003.

[8] L.H. Tenek and I. Hagiwara. Optimization of material distribution within isotropic and anisotropic plates using homogenization. *Comput. Methods Appl. Mech. Engrg.*, 109:155–167, 1992.

[9] L.H. Tenek and I. Hagiwara. Optimal rectangular plate and shallow shell topologies using thickness distribution or homogenization. *Comput. Methods Appl. Mech. Engrg.*, 115:111–124, 1994.

[10] A.R. Díaz, R. Lipton, and C.A. Soto. A new formulation of the problem of optimum reinforcement of reissner-mindlin plates. *Comput. Methods Appl. Mech. Engrg.*, 123:121–139, 1995.

[11] L.A. Krog and N. Olhoff. Optimum topology and reinforcement design of disk and plate structures with multiple stiffness and eigenfrequency objectives. *Computers and Structures*, 72:535–563, 1999.

[12] F. Belblidia, J.E.B. Lee, S. Rechak, and E. Hinton. Topology optimization of plate structures using single- or three-layered artificial material model. *Advances in Engineering Software*, 32:159–168, 2001.

[13] W. Kanok-Nukulchai. A simple and efficient finite element for general shell analysis. *Int. J. Numer. Meth. Engng.*, 14:179–200, 1979.

[14] N.L. Pedersen. Topology optimization of laminated plates with prestress. *Computers and Structures*, 80:559–570, 2002.

[15] C.S. Jog. Topology design of structures subjected to periodic loading. *Journal of Sound and Vibration*, 253:687–709, 2002.

[16] K.-J. Bathe. *Finite Element Procedures*. Prentice-Hall International, Inc., Upper Saddle River, New Jersey 07458, 1996.

[17] J. Stegmann and E. Lund. Nonlinear topology optimization of layered shell structures. *Struct. Multidisc. Optim.*, 29:349 – 360, 2005.

[18] R.D. Cook, D.S. Malkus, Plesha M.E., and R.J. Witt. *Concepts and applications of finite element analysis*. John Wiley and Sons, New York, 2002.

[19] T.J.R. Hughes and F. Brezzi. On drilling degrees of freedom. *Comput. Methods Appl. Mech. Engrg.*, 72:105–121, 1989.

[20] J.-L. Batoz and M. Ben Tahar. Evaluation of a new quadrilateral thin plate bending element. *Int. J. Numer. Meth. Engng.*, 18:1655–1677, 1982.

[21] O.C. Zienkiewicz and R.L. Taylor. *The Finite Element Method*, volume II: Solid and Fluid Mechanics Dynamics and Non-linearity. McGraw-Hill Book Company, London, 1991.

[22] K.-J. Bathe and E.N. Dvorkin. A four-node plate bending element based on Mindlin/Reissner plate theory and a mixed interpolation. *Int. J. Numer. Meth. Engng.*, 21:367–383, 1985.

[23] E. Dvorkin and K.-J. Bathe. A continuum mechanics based four node shell element for general nonlinear analysis. *Engineering Computations*, 1:77–88, 1984.

[24] O. Sigmund and J. Petersson. Numerical instabilities in topology optimization: A survey on procedures dealing with checkerboards, mesh-dependencies and local minima. *Struct. Multidisc. Optim.*, 16:68 – 75, 1998.

[25] O. Sigmund. On the design of compliant mechanisms using topology optimization. *Mechanics of Structures and Machines*, 25:495–526, 1997.

[26] A. Ibrahimbegovic, R.L. Taylor, and E.L. Wilson. A robust quadrilateral membrane finite element with drilling degrees of freedom. *Int. J. Numer. Meth. Engng.*, 30:445–457, 1990.

[27] O.C. Zienkiewicz, C.J. Parekh, and I.P. King. Arch dams analysed by a linear finite element shell solution program. In *Proc. Symp. on Theory of Arch Dams*, Southampton University, Pergamon Press, Oxford, 1965.

[28] A.A. Groenwold and N. Stander. An efficient 4-node 24 d.o.f. thick shell finite element with 5-point quadrature. *Engineering Computations*, 12:723–748, 1995.

[29] W.K. Liu, J.S-J Ong, and Uras R.A. Finite element stabilization matrices - A unification approach. *Comp. Meth. Applied Mech. Eng.*, 53:13–46, 1985.

[30] R.H. MacNeal. Derivation of element stiffness matrices by assumed strain distribution. *Nuclear Engineering Design*, 70:3–12, 1982.

[31] T.J.R. Hughes and T.E. Tezduyar. Finite elements based upon mindlin plate theory, with particular reference to the 4-node bilinear isoparametric element. *Journal of Applied Mechanics*, 48:587–595, 1981.

[32] R.L. Taylor. Finite element analysis of linear shell problems. In J.R. Whiteman, editor, *The Mathematics of Finite Elements and Applications VI, MAFELAP*, pages 191–203, Academic Press Limited, London, 1987.

[33] M.K. Rao and U. Shrinivasa. A set of pathological tests to validate new finite elements. *Sadhana*, 26:549–590, 2001.

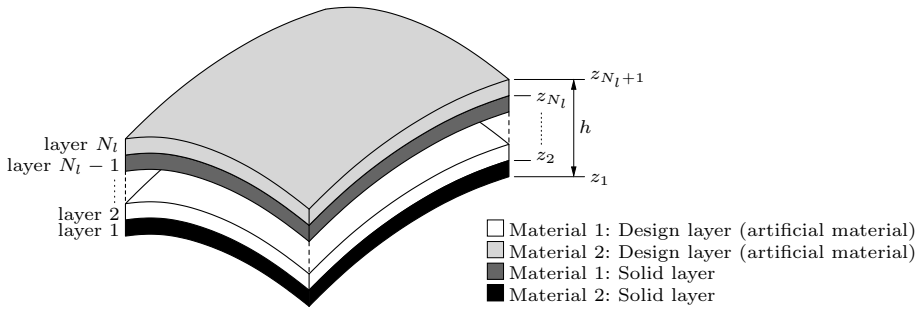

Fig. 1. A schematic representation of a general material layup for shell topology optimization problems.

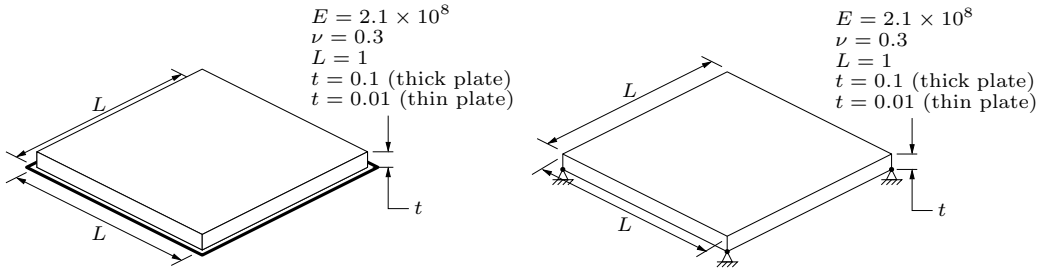

(a) Simply supported square plate. (b) Corner supported square plate.

Fig. 2. Example plate problems, geometry and constraints.

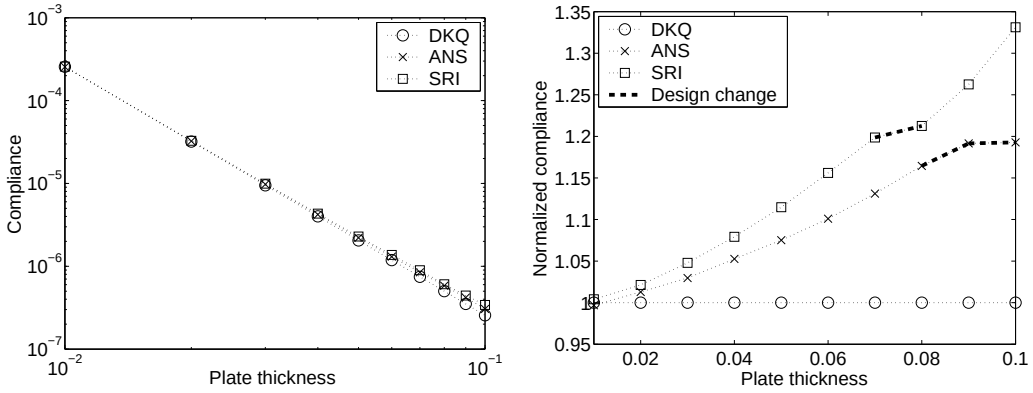

(a) Compliance on logarithmic scale. (b) Compliance normalized with respect to DKQ's cubic relation.

Fig. 3. Optimal topology compliance as a function of plate thickness for the simply supported plate subject to centre point load, single layer model.

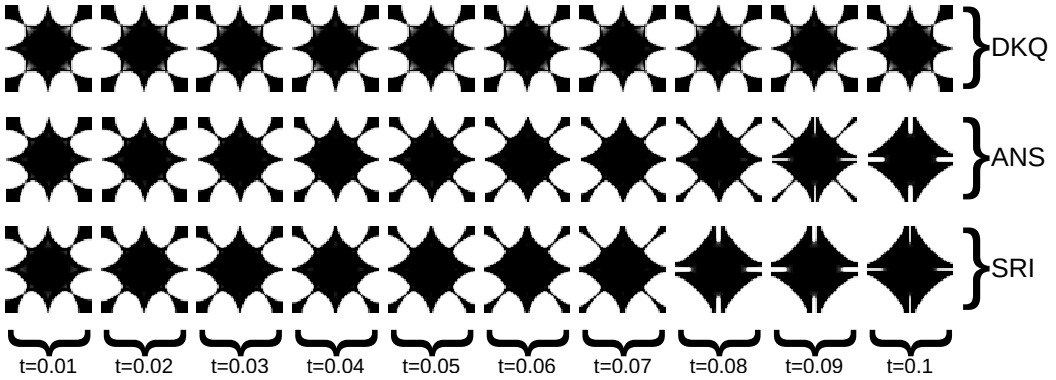

Fig. 4. Optimal topologies for various plate thicknesses, computed using different plate elements, of a simply supported plate subjected to center point load, single layer model.

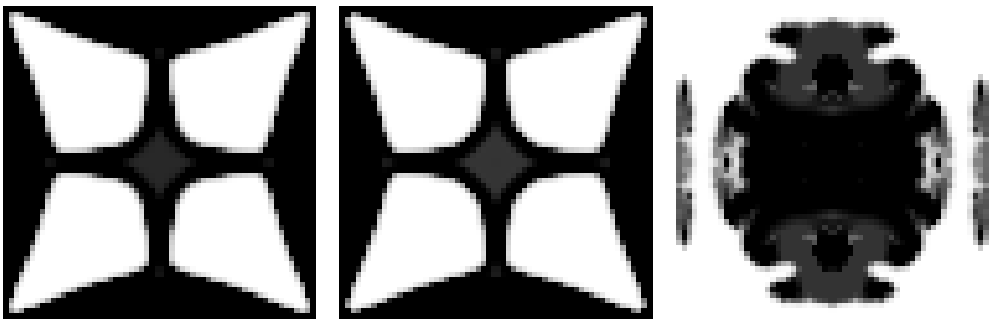

(a) Computed with DKQ elements. (b) Computed with ANS elements. (c) Computed with SRI elements.

Fig. 5. Optimal topologies of a corner supported square plate subjected to uniform distributed load, ribbed model, $t = 0.01$.

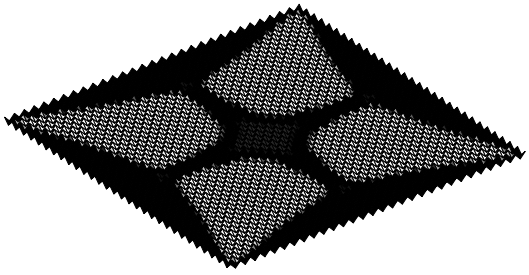

Fig. 6. Displaced shape of optimal topology computed using DKQ analyzed using SRI elements. Amplification factor 3×10^{-10}.

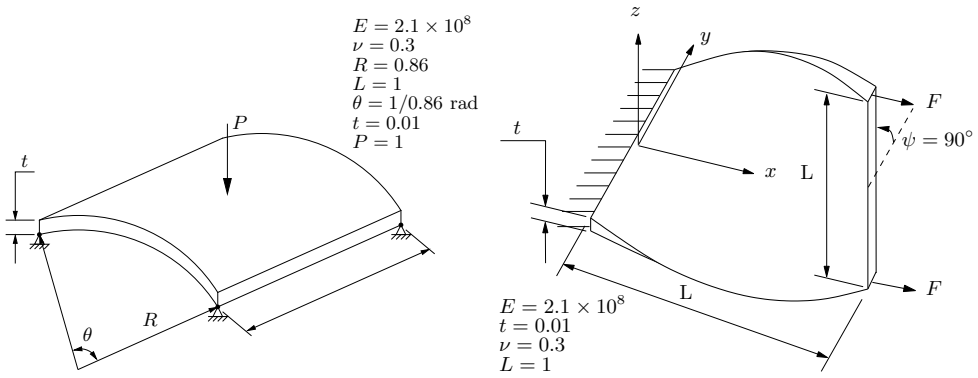

(a) Corner supported cylinder. (b) Pretwisted beam.

Fig. 7. Example shell problems, geometry and constraints.

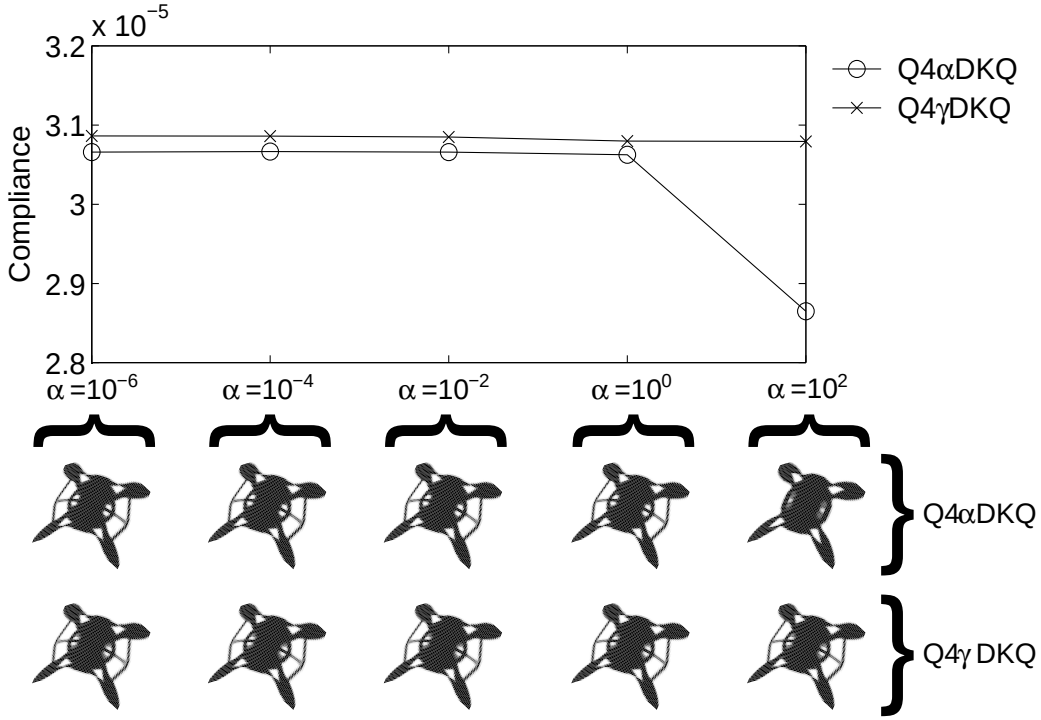

Fig. 8. Optimal topologies and associated compliance of a corner supported cylinder with single layer material model for various values of scaling factor α.

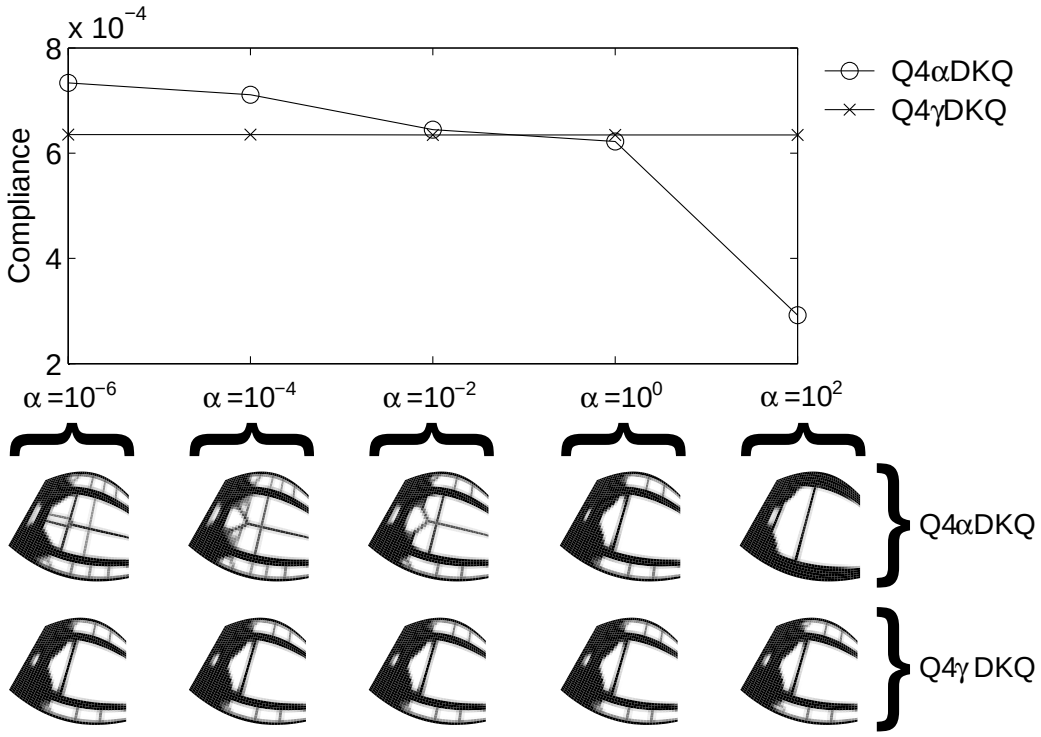

Fig. 9. Optimal topologies and associated compliance of a pretwisted beam with single layer material model for various values of scaling factor α.

	$\alpha = 10^{-6}$	$\alpha = 10^{-4}$	$\alpha = 10^{-2}$	$\alpha = 10^{0}$	$\alpha = 10^{2}$
Case 1	0.9943	0.9951	0.9956	0.9966	0.9795
Case 2	1.0054	1.0046	1.0041	1.0031	0.9996

Table 1
Corner supported cylinder: Compliance of optimal topology calculated using element A divided by the compliance of optimal topology calculated using element B, both evaluated using element A (α constant). Case 1: $A \equiv$Q4αDKQ, $B \equiv$Q4γDKQ. Case 2: $A \equiv$Q4γDKQ, $B \equiv$Q4αDKQ.

	$\alpha = 10^{-6}$	$\alpha = 10^{-4}$	$\alpha = 10^{-2}$	$\alpha = 10^{0}$	$\alpha = 10^{2}$
Case 1	0.9473	0.9588	0.9954	0.9989	0.9193
Case 2	0.9840	0.9831	0.9935	1.0007	0.8105

Table 2
Pretwisted beam: Compliance of optimal topology calculated using element A divided by the compliance of optimal topology calculated using element B, both evaluated using element A (α constant). Case 1: $A \equiv$Q4αDKQ, $B \equiv$Q4γDKQ. Case 2: $A \equiv$Q4γDKQ, $B \equiv$Q4αDKQ.